RESEARCH ARTICLE | JUNE 15 2023

Low intensity saturation of an ISB transition by a mid-IR quantum cascade laser

Mathieu Jeannin ; Eduardo Cosentino ; Stefano Pirotta; Mario Malerba ; Giorgio Biasiol ; Jean-Michel Manceau ; Raffaele Colombelli

Appl. Phys. Lett. 122, 241107 (2023)
https://doi.org/10.1063/5.0153891

Applied Physics Letters ARTICLE pubs.aip.org/aip/apl

Low intensity saturation of an ISB transition by a mid-IR quantum cascade laser

Cite as: Appl. Phys. Lett. **122**, 241107 (2023); doi: 10.1063/5.0153891
Submitted: 12 April 2023 · Accepted: 21 May 2023 ·
Published Online: 15 June 2023

Mathieu Jeannin,[1,a)] Eduardo Cosentino,[1] Stefano Pirotta,[1] Mario Malerba,[1] Giorgio Biasiol,[2] Jean-Michel Manceau,[1] and Raffaele Colombelli[1,a)]

AFFILIATIONS

[1]Centre de Nanosciences et de Nanotechnologies, CNRS UMR 9001, Université Paris Saclay, 10 Boulevard Thomas Gobert, 91120 Palaiseau, France
[2]Laboratorio TASC, CNR-IOM, Area Science Park, S.S. 14 km 163.5, Basovizza I-34149 Trieste, Italy

[a)]**Authors to whom correspondence should be addressed:** mathieu.jeannin@universite-paris-saclay.fr and raffaele.colombelli@universite-paris-saclay.fr

ABSTRACT

We demonstrate that absorption saturation of a mid-infrared intersubband transition can be engineered to occur at moderate light intensities of the order of 10–20 kW cm^{-2} and at room temperature. The structure consists of an array of metal–semiconductor–metal patches hosting a judiciously designed 253 nm thick GaAs/AlGaAs semiconductor heterostructure. At low incident intensity, the structure operates in the strong light–matter coupling regime and exhibits two absorption peaks at wavelengths close to 8.9 μm. Saturation appears as a transition to the weak coupling regime—and therefore, to a single-peaked absorption—when increasing the incident intensity. Comparison with a coupled mode theory model explains the data and permits to infer the relevant system parameters. When the pump laser is tuned at the cavity frequency, the reflectivity decreases with increasing incident intensity. When instead the laser is tuned at the polariton frequencies, the reflectivity non-linearly increases with increasing incident intensity. At those wavelengths, the system, therefore, mimics the behavior of a saturable absorption mirror in the mid-IR range, a technology that is currently missing.

Absorption saturation is one of the simplest non-linear optical process. In the case of interband transitions in semiconductors, it relies on Pauli blocking of photoexcited carriers, reducing the ability of the material to absorb light. This saturation process is, in general, governed by the lifetimes and oscillator strength of the involved transition and the frequency of the exciting light. Absorption saturation of interband transitions in semiconductors quantum wells (QWs) can be triggered with lasers at moderate intensities due to the long exciton lifetimes, which fill up the final states in the conduction band. Conversely, intersubband (ISB) transitions in doped QWs present very short (picosecond scale) lifetimes and typical low photon energy of tens or hundreds of milli-electronvolt. Contrary to interband transitions, absorption saturation of ISB transitions does not stem from a filling of the upper state of the transition, but from a depletion of the available carriers in the ground state whose density is fixed by the doping introduced in the structure. These characteristics leads to high saturation intensities, in the sub-megawatt per square centimeter range that are only attained with very high power lasers like CO_2 laser,[1] OPOs,[2–5] or even free electron lasers.[6] These high intensity values are, *in principle*, not compatible with conventional semiconductor lasers output powers, which has so far limited the application of ISB-based saturable absorbers. Some recent work mention saturation-like behavior of ISB transitions triggered using a simple quantum cascade lasers (QCLs), but in that case saturation was considered a drawback for non-linear light generation.[7,8]

ISB transitions are recognized for being a technological cornerstone in mid-infrared (mid-IR) optoelectronics, with the invention of the quantum cascade laser[9] that led to the development of practical mid-IR semiconductor lasers.[10] Since then, ISB transitions have contributed to the extension of semiconductor optoelectronic devices to the mid-IR and THz ranges of the electromagnetic spectrum. Examples are the demonstration and commercialization of mid-IR photodetectors,[11–15] free-space amplitude modulators.[16,17] As far as mid-IR saturable absorbers are concerned, initial results on narrow gap semiconductors[18] lead to recent efforts focused on finding new material systems relying, e.g., on type II superlattices[19] or two dimensional materials like graphene[20] and transition metal dichalcogenides[21] (see Refs. 22 and 23 for recent reviews). Hence, reducing the

absorption saturation intensity in ISB devices is technologically appealing as it would allow to exploit the design flexibility of ISB transitions to implement mid-IR saturable absorbers. Demonstrating low-intensity saturation of an ISB-based devices is, therefore, an important first step.

In a recent theoretical work, we have developed a unified formalism to describe absorption saturation of ISB transitions coupled to microcavities.[24] In particular, we have shown that the nature of absorption saturation radically changes in cavity-coupled systems depending on the light–matter interaction regime, quantified by the vacuum Rabi frequency Ω_R,

$$\Omega_R^2 = f_w f_{12} \frac{\Delta n\, e^2}{4\varepsilon\varepsilon_0 m^* L_{qw}} \equiv a\Delta n, \tag{1}$$

where f_w is the filling fraction of the QWs inside the active region, f_{12} is the transition oscillator strength hereafter approximated to the infinite square QW limit ($f_{12} = 0.96$), e and m^* are the electron charge and effective mass, ε_0 and ε are the vacuum permittivity and the semiconductor relative permittivity, L_{qw} is the QW width, and $\Delta n = n_1 - n_2$ is the population difference between the first (n_1) and the second (n_2) electronic levels of the QW. The absorption saturation manifests itself with the collapse of the light–matter coupling as both Δn, and thus, Ω_R, tend to zero.

In this work, we experimentally demonstrate that the absorption saturation of mid-IR intersubband transitions can be drastically reduced down to the kilowatt per square centimeter range. Such low values are compatible with the output power of commercially available quantum cascade lasers (QCLs), interband cascade lasers (ICLs), and emerging mid-IR fiber lasers.[25,26] The saturation intensity I_{sat} is defined as the intensity for which the population difference Δn is reduced to half the value of the introduced doping n_s, or—equivalently—the population in the excited level is $n_s/4$,

$$\Delta n_{I_{sat}} = \frac{n_s}{2} \iff n_{2,sat} = \frac{n_s}{4}. \tag{2}$$

To achieve saturation with a low incident intensity, a careful balance has to be found. Following Ref. 24, structures with low doping can exhibit low saturation intensities when introduced in a properly designed cavity. However, if the doping is so small that the polariton splitting cannot be resolved, the spectral signature of the saturation is masked by the cavity absorption. Increasing the doping allows to increase the frequency splitting, but leads to a linear increase in saturation intensity as $I_{sat} \propto \Omega_R^2$. The best choice is, therefore, to operate at the onset of the strong light–matter coupling regime, where a moderate Ω_R allows to spectrally resolve the polariton states while retaining a low I_{sat}. This constitutes a first steps toward a unique semiconductor saturable absorber mirror[27–29] (SESAM) technology that could have great impact for mid-IR lasers.

We have designed a saturable absorber active region composed of seven repetitions of GaAs/$Al_{0.33}Ga_{0.67}As$ QWs (6.5/14 nm, total thickness 253 nm) delta-doped with Si atoms with surface density of $2 \times 10^{11}\,cm^{-2}$ (sample HM4448). Additional delta-doping layers on each side of the multi-QW structure are introduced to compensate for Fermi level pinning at the semiconductor–metal interfaces. A reference sample (HM4445) with the same, but undoped, active region has also been fabricated to measure the optical response of the bare cavity. The active region is processed using standard Au–Au thermocompressive wafer bonding,[30] selective substrate removal in citric acid, and electron beam lithography to fabricate arrays of metal–metal patch cavities, as shown in Fig. 1(a). The semiconductor between adjacent Au patches is removed by ICP-RIE using $SiCl_4$. A self-consistent Schrödinger–Poisson simulation [Fig. 1(b)] shows the conduction band profile and confined electronic states of the QWs, with an energy separation of 138 meV corresponding to a transition wavenumber of $1110\,cm^{-1}$ ($\lambda \approx 9\,\mu m$). The patch cavity size s ranges from 1.25 to 1.35 μm to tune the frequency of the fundamental TM_{00} [Fig. 1(c)] mode across the ISB transition. The distance p between adjacent cavities is fixed at $p = 1\,\mu m$ to operate close to the critical coupling condition, ensuring maximal energy funneling in the system.

The samples are initially characterized in a Fourier-transform infrared (FTIR) spectrometer equipped with a Cassegrain microscope objective, to measure the reflectivity spectrum of each cavity array. The results are shown in Fig. 2(a) for both the undoped QW sample (purple dashed lines) and the doped QW sample (blue solid line). The undoped sample exhibits a single absorption dip, corresponding to Ohmic dissipation in the cavity. The absorption frequency ω_c decreases with increasing patch size s following the usual relation:

$$\omega_c = \frac{\pi c}{n_{eff}\, s}, \tag{3}$$

where n_{eff} is an effective refractive index. On the contrary, the reflectivity spectra of the doped QWs sample exhibit two absorption dips, on each side of the bare cavity absorption, as highlighted in the inset of Fig. 2. We fit the datasets with Lorentzian absorption lines and report

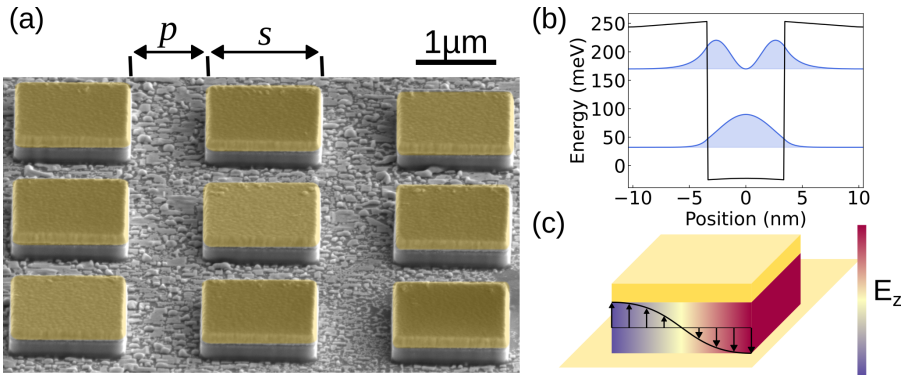

FIG. 1. (a) Colorized SEM image of a typical patch antenna array defining the dimensions s and p. (b) Self-consistent Schrödinger–Poisson simulation of a period of the structure showing the two confined electronic states. (c) Sketch of a single patch antenna with the electric field amplitude of the fundamental TM_{00} mode.

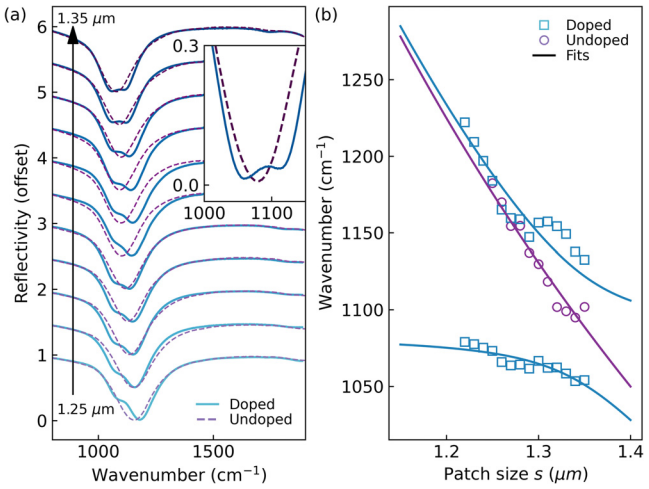

FIG. 2. (a) Reflectivity of the bare cavity arrays (purple dashed line) and of the doped cavity arrays (blue solid lines) as a function of the cavity size. The spectra are offset by 0.5. Inset: zoom on the $s = 1.35\,\mu$m spectrum around the polariton splitting. (b) Cavity and polaritons dispersion relation as a function of the patch size. The symbols are the experimental data (circles: undoped cavities and squares: doped cavities) extracted from Lorentzian fits of the spectra. The solid lines are fit to Eqs. (3) and (4), respectively.

the extracted peak frequencies as a function of patch size s in Fig. 2(b) (open symbols). The two absorption dips in the doped QWs sample exhibit an anti-crossing behavior, characteristic of the strong light–matter coupling regime. The low (respectively, high) frequency branch corresponds to the lower (respectively, upper) polariton. First, the dispersion relation of the (undoped) cavity is fitted (purple solid line) according to Eq. (3), providing $n_{eff} = 3.5$, slightly larger than $n_{GaAs} \approx 3.3$ at these frequencies. This stems from the strong confinement of the electric field between the two metallic plates, together with field leakage and reflection phase at the edges of the cavity. Then, the dispersion relation of the polariton branches is fitted using the following secular equation:[31]

$$\left(\omega^2 - \omega_{isb}^2\right)\left(\omega^2 - \omega_c^2\right) = 4\Omega_R^2\omega_c^2, \tag{4}$$

where ω_{isb} is the intersubband transition frequency and ω_c is the cavity frequency. In the limit of very low excitation, we can replace $\Delta n \approx n_s$ in the expression of the Rabi frequency.

The slight discrepancy between the secular equation (4) and the data can have several causes, e.g., differences in the fabrication of the two samples resulting in actual patch sizes s slightly different between the two samples. To correct for this effect, we assign the cavities sizes by comparing the frequency of their higher order modes (unperturbed by the ISB transition). From the fit, we extract a Rabi splitting of $2\Omega_R = 70$ cm^{-1}, which is slightly below the minimal splitting of 78 cm^{-1} measured in the $s = 1.35\,\mu$m cavity case. These values should be compared with the resonance frequency and the cavity/ISB transition linewidths (respectively, γ_c^{tot} and γ_{isb}^{tot}), yielding $\frac{\Omega_R}{\omega_{isb}} = 0.04$ and $\frac{2\Omega_R}{\gamma_{c,isb}^{tot}} = 0.65$. The Rabi frequency is only a fraction of the transition frequency, but the Rabi splitting is of the order of the dissipation rates of the system. This places the system *de facto* at the onset of the strong light–matter coupling regime, as we can still resolve the polariton splitting.

We then measure the non-linear reflectivity of the doped QWs array closest to resonance ($s = 1.35\,\mu$m) as a function of the excitation intensity. The reflectivity is probed with a home-built microscope setup using a commercial tunable QCL (Daylight MIRCAT) as a source and a liquid-nitrogen cooled mercury cadmium telluride detector.[16] The QCL emission is amplitude modulated at 10 kHz with pulse widths of 500 ns (0.5% duty cycle), and lock-in detection is employed. The incident intensity can be tuned through a half-wave plate and a polarizer and with the laser injection current (see the supplementary material for a complete description). The reflectivity of the patch cavity array is normalized against that of a smooth Au surface. Figure 3(a) reports the reflectivity spectra of the sample at low intensity (blue symbols) as well as at the maximum intensity available from the QCL (purple symbols). For low impinging intensity, we retrieve the two absorption dips [inset of Fig. 2(a)] with two polariton states. On the contrary, the high intensity spectrum displays only one absorption dip, centered between the two polariton states.

We then select three frequencies from the spectrum in Fig. 3(a). The cavity central frequency (1080 cm^{-1}, purple arrow), the upper polariton frequency (1112 cm^{-1}, light blue arrow), and the frequency at which the reflectivity change is the largest (1140 cm^{-1}, black arrow). Note that the latter frequency accidentally lies at the crossover between two QCL chips, hence the small jump in the high intensity reflectivity spectrum. With the laser tuned at these three frequencies, we continuously scan the incident intensity. The value of the exciting power (in milliwatt) is measured using a thermoelectric detector, and the spot size (20 μm radius at 1/e^2) is determined with a knife-edge measurement to infer the excitation intensity (in watt per square centimeter).

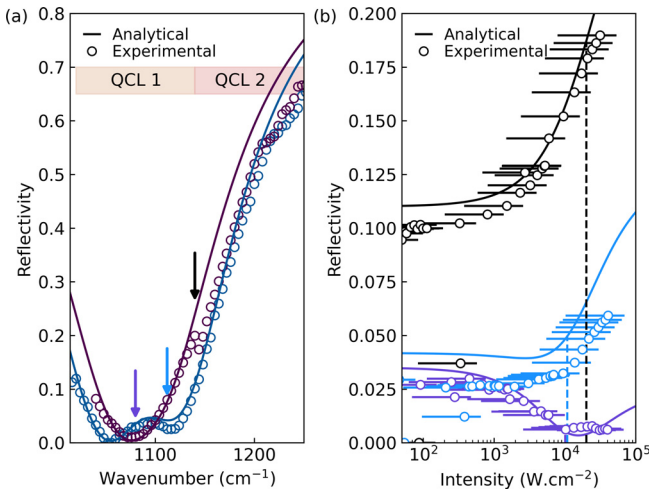

FIG. 3. (a) Reflectivity spectra of the doped $s = 1.35\,\mu$m cavity array under low (purple circles) and high (blue circles) intensity excitation. The shaded areas indicate the tuning ranges of the QCL chips. (b) Nonlinear reflectivity as a function of intensity for three different wavelengths [arrows in (a)]. Open symbols correspond to experimental data, and solid lines to the CMT prediction. The vertical dashed lines indicate the saturation condition. The horizontal error bars represent uncertainty on the evaluation of the spot size.

The results are presented in Fig. 3(b) (open symbols). Pumping within the polariton gap at the cavity frequency leads to a decrease in reflectivity as the transition saturates, and the response of the system converges to the one of the bare cavity. On the contrary, pumping at the upper polariton frequency or on the high frequency edge of the spectrum leads to a gradual increase in reflectivity.

We use temporal coupled mode theory (CMT) to obtain an analytical expression relating the sample reflectivity (and the population difference Δn) to the incident laser intensity. The ISB transition and the cavity mode are modeled as oscillators with parameters $(\omega_i, \gamma_i, \Gamma_i)$ representing, respectively, their oscillation frequency, non-radiative, and radiative dampings. In the present case, the radiative coupling of the ISB transition to free-space radiation ($\Gamma_{isb} = 0$) can be neglected.[32,33] The three equations describing the evolution of the amplitude a_i of each oscillator, as well as the in- and outcoupling equation of the exciting field s^+ and s^- are, thus,[24]

$$\frac{da_{isb}}{dt} = (i\omega_{isb} - \gamma_{isb})a_{isb} + i\Omega_R a_c, \tag{5}$$

$$\frac{da_c}{dt} = (i\omega_c - \gamma_{nr} - \Gamma_r)a_c + i\Omega_R a_{isb} + \sqrt{2\Gamma_r}s^+, \tag{6}$$

$$s^- = -s^+ + \sqrt{2\Gamma_r}a_c, \tag{7}$$

which can be solved in the harmonic regime ($s^+ = e^{i\omega t}$) to express analytically the absorption $\mathcal{A}_{isb} = 2\gamma_{isb}|\frac{a_{isb}}{s^+}|^2$ solely due to the ISB transition, and the reflectivity $R = |\frac{s^-}{s^+}|^2$. Assuming (without loss of generality) that the cavity is at resonance with the ISB transition, i.e., $\omega_c = \omega_{isb} = \omega_0$, we have

$$\mathcal{A}_{isb}(\Delta n) = \frac{4\gamma_{isb}\Gamma_r\Omega_R^2}{\left[(\omega-\omega_0)^2 - \Omega_R^2 - \gamma_{isb}(\gamma_{nr}+\Gamma_r)\right]^2 + \left[(\gamma_{nr}+\Gamma_r+\gamma_{isb})(\omega-\omega_0)\right]^2}, \tag{8}$$

$$R(\Delta n) = \frac{\left[(\omega-\omega_0)^2 - \Omega_R^2 + \gamma_{isb}(\Gamma_r-\gamma_{nr})\right]^2 + \left[(\Gamma_r-\gamma_{nr}-\gamma_{isb})(\omega-\omega_0)\right]^2}{\left[(\omega-\omega_0)^2 - \Omega_R^2 - \gamma_{isb}(\gamma_{nr}+\Gamma_r)\right]^2 + \left[(\gamma_{nr}+\Gamma_r+\gamma_{isb})(\omega-\omega_0)\right]^2}. \tag{9}$$

These expressions directly depend on the population difference Δn through the Rabi frequency (1). We then link the excited state excited population of the ISB transition n_2 in steady-state condition under an incident intensity I using

$$n_2 = \frac{I}{N_{qw}\hbar\omega}\tau_{12}\mathcal{A}_{isb}(\Delta n), \tag{10}$$

where τ_{12} is the upper state lifetime (of the order of the ps) and N_{qw} is the number of QWs. Inserting Eq. (8) in Eq. (10) leads—after inversion—to the following intensity-dependent excited state population:[34]

$$I = \frac{\hbar\omega N_{qw}}{4\tau_{12}}\frac{n_2\left[\left[\gamma_{isb}(\gamma_{nr}+\Gamma_r) - \left((\omega-\omega_0)^2 - a(n_s-2n_2)\right)\right]^2 + (\omega-\omega_0)^2(\gamma_{isb}+\gamma_{nr}+\Gamma_r)^2\right]}{\gamma_{isb}\Gamma_r a(n_s-2n_2)}, \tag{11}$$

where the coefficient a has been defined in Eq. (1). Importantly, using (9), this result allows us to establish a correspondence between the incident intensity and the measured non-linear reflectivity variation through the excited state population.

All the experimental results (reflectivity spectra and non-linear reflectivity curves) are fitted by combining Eqs. (9) and (11) and using a single set of parameters. The results are presented as solid lines in Fig. 3. The total quality factor $Q_c^{tot} = \frac{\omega_c}{2(\Gamma_r+\gamma_{nr})} = 6$ and the electronic doping $n_s = 2\times10^{11}$ cm^{-2} are obtained from the experiment: the former one from the experimental total cavity linewidth of the undoped sample [Fig. 2(a)], and the latter one from the experimental value of the Rabi frequency using Eq. (1). The only free parameters are the ratio between the radiative and non-radiative cavity dissipation rates, and the ISB linewidth γ_{isb}. The fit yields $Q_r = 9.5 \pm 0.3$ and $Q_{nr} = 13 \pm 0.1$, and $Q_{isb} = 13 \pm 0.7$. The analytical results are presented in solid lines in Fig. 3.

The calculations quantitatively reproduce all features of the experimental data. We observe the collapse of the polariton states from the low intensity to the high intensity reflectivity spectra. We also observe the decrease in the non-linear reflectivity as a function of intensity when pumping in the gap, and the increase in the non-linear reflectivity when pumping at the polariton frequency or on the high frequency edge. In particular Eq. (11) permits to deduce the excited state population from the non-linear reflectivity curves, an information that cannot be extracted from the sole measurements. This allows us to mark the saturation condition (2), shown in vertical dashed lines in Fig. 3(b). Depending on the pump frequency, saturation is achieved for intensities of 10–20 kW cm^{-2}.

We now examine the limitations of the model and its agreement with the experimental data. A first approximation is made when considering that the ISB transition frequency does not depend on the saturation of the transition. In reality, collective effects in confined electron gas renormalize the transition energy through the depolarization shift, according to the following formula:

$$\omega_{isb}^2(\Delta n) = \omega_{isb,0}^2 + \frac{e^2}{\varepsilon\varepsilon_0 m^* L_{qw}}\Delta n, \tag{12}$$

where the square root of the last operand on the right-hand-side is known as the plasma frequency. In mid-IR delta-doped QWs, and at

such moderates dopings, the depolarization shift is small.[35] The validity of this approximation is gauged *a posteriori* by the quantitative agreement between theory and experimental results. This effect should be considered at larger doping densities or in the case of THz ISB transition where the depolarization shift is generally a larger fraction of the transition energy.[36,37]

On the experimental side, we identify two main limitations. The first one is the non-homogeneous excitation of the patch cavity array by the (Gaussian) laser beam: all the cavities probed by the beam actually experience different excitation intensities and, thus, exhibit different reflectivity spectra, possibly resulting in a broadening of the response. The second limitation is the precise determination of the pump spot size. Given the moderate output power of the QCL, a strong focusing is needed to reach high enough intensities. Even when performed with great care, knife-edge measurements of the focal spot size are difficult and can lead to variations in the intensity inferred from the power measurement, as shown by the error bars in Fig. 3(b).

Finally, since the sample is excited using relatively long laser pulses, it is important to estimate the importance of thermal effects in the structure and, in particular, to estimate whether the observed effect could simply be a manifestation of heating. We report in the supplementary material an estimation of thermal effects, showing that the nonlinear reflectivity change reported here is indeed due to absorption saturation.

In conclusion, we have demonstrated absorption saturation of an ISB transition at a record low intensity (10–20 kW cm^{-2}) by a judicious engineering of the light–matter coupling, making it compatible with mid-IR semiconductor lasers. The measured non-linear reflectivity properties have validated the analytical model of saturation in weak and strong-coupling regime that we had developed in Ref. 24. This result constitutes a first step toward semiconductor saturable absorber mirrors (SESAM) able to cover the mid-IR spectral range. To further improve this system, future work will focus on improving the main figures of merit of the device: saturation intensity, reflectivity contrast, and non-saturable losses. Furthermore, given the fast decoherence times of the order of hundreds of femtoseconds,[38] and the fast population relaxation times of the order of a few picoseconds[2,3,5,39,40] of ISB transitions confirmed in recent demonstration of final state stimulation of ISB polaritons,[41] we expect fast saturation and recovery dynamics on the order of few ps.[42] We conclude by emphasizing that this approach is in principle intrinsically scalable to the full mid-IR range. ISB transitions in III–V semiconductors are well mastered and can cover the entire mid-infrared. The cavity electrodynamics concepts enabling the observed ultra-low intensity saturation are also fully scalable to other wavelengths. We, therefore, believe that this experimental demonstration represents the first step toward a robust technology for mid-infrared SESAMs. It could have impact for mid-IR lasers, judging from the success SESAMs had at shorter near-infrared wavelengths.[27–29]

See the supplementary material for a complete description of the non-linear reflectivity setup and an estimation of thermal effects in the structure.

This work was partially supported by the European Union Future and Emerging Technologies (FET) Grant No. 737017 (MIRBOSE) and by the French National Research Agency: Project SOLID (No. ANR-19-CE24-0003) and IRENA (No. ANR-17-CE24-0016). This work was partly supported by the RENATECH network and the General Council of Essonne. M.M. acknowledges the support from the Marie Skłodowska Curie Action, Grant Agreement No. 748071. We acknowledge the technical help of the C2N cleanroom staff. We thank Iacopo Carusotto, Ammar Hideur, and Adel Bousseksou for scientific discussions, Cristiano Ciuti for granting us access to the Laboratoire Matériaux et Phénomènes Quantiques cleanroom (CNRS UMR 7162, Université Paris-Cité), and Pascal Filloux for assistance in the ICP-RIE etching of the structures.

AUTHOR DECLARATIONS

Conflict of Interest

The authors have no conflicts to disclose.

Author Contributions

Mathieu Jeannin: Conceptualization (lead); Formal analysis (lead); Investigation (lead); Software (lead); Supervision (lead); Writing – original draft (lead); Writing – review & editing (lead). **Eduardo Cosentino:** Investigation (supporting); Writing – original draft (supporting); Writing – review & editing (supporting). **Stefano Pirotta:** Investigation (supporting); Resources (equal); Writing – original draft (supporting); Writing – review & editing (supporting). **Mario Malerba:** Resources (supporting); Writing – original draft (supporting); Writing – review & editing (supporting). **Giorgio Biasiol:** Investigation (supporting); Resources (lead); Writing – original draft (supporting); Writing – review & editing (supporting). **Jean-Michel Manceau:** Conceptualization (equal); Investigation (equal); Supervision (equal); Writing – original draft (lead); Writing – review & editing (lead). **Raffaele Colombelli:** Conceptualization (lead); Funding acquisition (lead); Resources (lead); Supervision (lead); Writing – original draft (lead); Writing – review & editing (lead).

DATA AVAILABILITY

The data that support the findings of this study are available from the corresponding authors upon reasonable request.

REFERENCES

[1]F. H. Julien, J.-M. Lourtioz, N. Herschkorn, D. Delacourt, J. P. Pocholle, M. Papuchon, R. Planel, and G. Le Roux, "Optical saturation of intersubband absorption in GaAs-Al_xGa_{1-x}As quantum wells," Appl. Phys. Lett. **53**, 116–118 (1988).

[2]A. Seilmeier, H.-J. Hübner, G. Abstreiter, G. Weimann, and W. Schlapp, "Intersubband relaxation in GaAs-Al_xGa_{1-x}As quantum well structures observed directly by an infrared bleaching technique," Phys. Rev. Lett. **59**, 1345–1348 (1987).

[3]K. L. Vodopyanov, V. Chazapis, C. C. Phillips, B. Sung, and J. S. Harris, "Intersubband absorption saturation study of narrow III - V multiple quantum wells in the $\lambda = 2.8$–9 μm spectral range," Semicond. Sci. Technol. **12**, 708–714 (1997).

[4]S. Zanotto, R. Degl'Innocenti, J.-H. Xu, L. Sorba, A. Tredicucci, and G. Biasiol, "Ultrafast optical bleaching of intersubband cavity polaritons," Phys. Rev. B **86**, 201302 (2012).

[5]S. A. Mann, N. Nookala, S. C. Johnson, M. Cotrufo, A. Mekawy, J. F. Klem, I. Brener, M. B. Raschke, A. Alù, and M. A. Belkin, "Ultrafast optical switching and power limiting in intersubband polaritonic metasurfaces," Optica **8**, 606 (2021).

[6]M. Helm, T. Fromherz, B. N. Murdin, C. R. Pidgeon, K. K. Geerinck, N. J. Hovenyer, W. T. Wenckebach, A. F. G. van der Meer, and P. W. van Amersfoort, "Complete bleaching of the intersubband absorption in GaAs/AlGaAs quantum wells using a far-infrared free-electron laser," Appl. Phys. Lett. **63**, 3315–3317 (1993).
[7]J. Lee, M. Tymchenko, C. Argyropoulos, P.-Y. Chen, F. Lu, F. Demmerle, G. Boehm, M.-C. Amann, A. Alù, and M. A. Belkin, "Giant nonlinear response from plasmonic metasurfaces coupled to intersubband transitions," Nature **511**, 65–69 (2014).
[8]J. S. Gomez-Diaz, M. Tymchenko, J. Lee, M. A. Belkin, and A. Alù, "Nonlinear processes in multi-quantum-well plasmonic metasurfaces: Electromagnetic response, saturation effects, limits, and potentials," Phys. Rev. B **92**, 125429 (2015).
[9]J. Faist, *Quantum Cascade Lasers* (Oxford University Press, Oxford, 2018).
[10]A. Baranov and E. Tournié, *Semiconductor Lasers: Fundamentals and Applications* (Elsevier, 2013).
[11]H. Schneider and H. C. Liu, *Quantum Well Infrared Photodetectors: Physics and Applications*, Springer Series in Optical Sciences Vol. 126 (Springer, Berlin, New York, 2007).
[12]M. Hakl, Q. Lin, S. Lepillet, M. Billet, J.-F. Lampin, S. Pirotta, R. Colombelli, W. Wan, J. C. Cao, H. Li, E. Peytavit, and S. Barbieri, "Ultrafast quantum-well photodetectors operating at 10 μm with a flat frequency response up to 70 GHz at room temperature," ACS Photonics **8**, 464–471 (2021).
[13]J. Hillbrand, L. M. Krüger, S. D. Cin, H. Knötig, J. Heidrich, A. M. Andrews, G. Strasser, U. Keller, and B. Schwarz, "High-speed quantum cascade detector characterized with a mid-infrared femtosecond oscillator," Opt. Express **29**, 5774–5781 (2021).
[14]M. Lagrée, M. Jeannin, G. Quinchard, O. Ouznali, A. Evirgen, V. Trinité, R. Colombelli, and A. Delga, "Direct polariton-to-electron tunneling in quantum cascade detectors operating in the strong light-matter coupling regime," Phys. Rev. Appl. **17**, 044021 (2022).
[15]G. Quinchard, C. Mismer, M. Hakl, J. Pereira, Q. Lin, S. Lepillet, V. Trinité, A. Evirgen, E. Peytavit, J. L. Reverchon, J. F. Lampin, S. Barbieri, and A. Delga, "High speed, antenna-enhanced 10.3 μm quantum cascade detector," Appl. Phys. Lett. **120**, 091108 (2022).
[16]S. Pirotta, N.-L. Tran, A. Jollivet, G. Biasiol, P. Crozat, J.-M. Manceau, A. Bousseksou, and R. Colombelli, "Fast amplitude modulation up to 1.5 GHz of mid-IR free-space beams at room-temperature," Nat. Commun. **12**, 799 (2021).
[17]H. Dely, T. Bonazzi, O. Spitz, E. Rodriguez, D. Gacemi, Y. Todorov, K. Pantzas, G. Beaudoin, I. Sagnes, L. Li, A. G. Davies, E. H. Linfield, F. Grillot, A. Vasanelli, and C. Sirtori, "10 Gbit s^{-1} free space data transmission at 9 μm wavelength with unipolar quantum optoelectronics," Laser Photonics Rev. **16**, 2100414 (2022).
[18]K. L. Vodopyanov, A. V. Lukashev, C. C. Phillips, and I. T. Ferguson, "Passive mode locking and Q switching of an erbium 3 μm laser using thin InAs epilayers grown by molecular beam epitaxy," Appl. Phys. Lett. **59**, 1658–1660 (1991).
[19]Z. Qin, X. Chai, G. Xie, Z. Xu, Y. Zhou, Q. Wu, J. Li, Z. Wang, Y. Weng, T. Hai, P. Yuan, J. Ma, J. Chen, and L. Qian, "Semiconductor saturable absorber mirror in the 3–5 μm mid-infrared region," Opt. Lett. **47**, 890 (2022).
[20]Q. Bao, H. Zhang, Y. Wang, Z. Ni, Y. Yan, Z. X. Shen, K. P. Loh, and D. Y. Tang, "Atomic-layer graphene as a saturable absorber for ultrafast pulsed lasers," Adv. Funct. Mater. **19**, 3077–3083 (2009).
[21]Y. Tan, X. Liu, Z. He, Y. Liu, M. Zhao, H. Zhang, and F. Chen, "Tuning of interlayer coupling in large-area graphene/WSe_2 van der Waals heterostructure via ion irradiation: Optical evidences and photonic applications," ACS Photonics **4**, 1531–1538 (2017).
[22]J. Ma, Z. Qin, G. Xie, L. Qian, and D. Tang, "Review of mid-infrared mode-locked laser sources in the 2.0 μm–3.5 μm spectral region," Appl. Phys. Rev. **6**, 021317 (2019).
[23]G. Liang, X. Yu, X. Hu, B. Qiang, C. Wang, and Q. J. Wang, "Mid-infrared photonics and optoelectronics in 2D materials," Mater. Today **51**, 294–316 (2021).
[24]M. Jeannin, J.-M. Manceau, and R. Colombelli, "Unified description of saturation and bistability of intersubband transitions in the weak and strong light-matter coupling regimes," Phys. Rev. Lett. **127**, 187401 (2021).
[25]R. I. Woodward, M. R. Majewski, and S. D. Jackson, "Mode-locked dysprosium fiber laser: Picosecond pulse generation from 2.97 to 3.30 μm," APL Photonics **3**, 116106 (2018).
[26]M. R. Majewski, R. I. Woodward, J.-Y. Carreé, S. Poulain, M. Poulain, and S. D. Jackson, "Emission beyond 4 μm and mid-infrared lasing in a dysprosium-doped indium fluoride (InF_3) fiber," Opt. Lett. **43**, 1926–1929 (2018).
[27]U. Keller, D. A. B. Miller, G. D. Boyd, T. H. Chiu, J. F. Ferguson, and M. T. Asom, "Solid-state low-loss intracavity saturable absorber for Nd:YLF lasers: An antiresonant semiconductor Fabry–Perot saturable absorber," Opt. Lett. **17**, 505 (1992).
[28]U. Keller, K. Weingarten, F. Kartner, D. Kopf, B. Braun, I. Jung, R. Fluck, C. Honninger, N. Matuschek, and J. Aus der Au, "Semiconductor saturable absorber mirrors (SESAM's) for femtosecond to nanosecond pulse generation in solid-state lasers," IEEE J. Sel. Top. Quantum Electron. **2**, 435–453 (1996).
[29]U. Keller, "Recent developments in compact ultrafast lasers," Nature **424**, 831–838 (2003).
[30]J.-M. Manceau, N.-L. Tran, G. Biasiol, T. Laurent, I. Sagnes, G. Beaudoin, S. De Liberato, I. Carusotto, and R. Colombelli, "Resonant intersubband polariton-LO phonon scattering in an optically pumped polaritonic device," Appl. Phys. Lett. **112**, 191106 (2018).
[31]Y. Todorov, A. M. Andrews, R. Colombelli, S. De Liberato, C. Ciuti, P. Klang, G. Strasser, and C. Sirtori, "Ultrastrong light-matter coupling regime with polariton dots," Phys. Rev. Lett. **105**, 196402 (2010).
[32]F. Alpeggiani and L. C. Andreani, "Semiclassical theory of multisubband plasmons: Nonlocal electrodynamics and radiative effects," Phys. Rev. B **90**, 115311 (2014).
[33]M. Jeannin, T. Bonazzi, D. Gacemi, A. Vasanelli, L. Li, A. G. Davies, E. Linfield, C. Sirtori, and Y. Todorov, "Absorption engineering in an ultrasubwavelength quantum system," Nano Lett. **20**, 4430–4436 (2020).
[34]A. Baas, J. P. Karr, H. Eleuch, and E. Giacobino, "Optical bistability in semiconductor microcavities," Phys. Rev. A **69**, 023809 (2004).
[35]R. Cominotti, H. A. M. Leymann, J. Nespolo, J.-M. Manceau, M. Jeannin, R. Colombelli, and I. Carusotto, "Theory of coherent optical nonlinearities of intersubband transitions in semiconductor quantum wells," Phys. Rev. B **107**, 115431 (2023).
[36]M. Załużny, "Influence of the depolarization effect on the nonlinear intersubband absorption spectra of quantum wells," Phys. Rev. B **47**, 3995–3998 (1993).
[37]K. Craig, B. Galdrikian, J. N. Heyman, A. G. Markelz, J. B. Williams, M. S. Sherwin, K. Campman, P. F. Hopkins, and A. C. Gossard, "Undressing a collective intersubband excitation in a quantum well," Phys. Rev. Lett. **76**, 2382–2385 (1996).
[38]R. A. Kaindl, K. Reimann, M. Woerner, T. Elsaesser, R. Hey, and K. H. Ploog, "Homogeneous broadening and excitation-induced dephasing of intersubband transitions in a quasi-two-dimensional electron gas," Phys. Rev. B **63**, 161308 (2001).
[39]S. Lutgen, R. A. Kaindl, M. Woerner, T. Elsaesser, A. Hase, and H. Künzel, "Nonlinear intersubband absorption of a hot quasi-two-dimensional electron plasma studied by femtosecond infrared spectroscopy," Phys. Rev. B **54**, R17343–R17346 (1996).
[40]S. Lutgen, R. A. Kaindl, M. Woerner, T. Elsaesser, A. Hase, H. Künzel, M. Gulia, D. Meglio, and P. Lugli, "Nonequilibrium dynamics in a quasi-two-dimensional electron plasma after ultrafast intersubband excitation," Phys. Rev. Lett. **77**, 3657–3660 (1996).
[41]M. Knorr, J. M. Manceau, J. Mornhinweg, J. Nespolo, G. Biasiol, N. L. Tran, M. Malerba, P. Goulain, X. Lafosse, M. Jeannin, M. Stefinger, I. Carusotto, C. Lange, R. Colombelli, and R. Huber, "Intersubband polariton-polariton scattering in a dispersive microcavity," Phys. Rev. Lett. **128**, 247401 (2022).
[42]J. Raab, C. Lange, J. L. Boland, I. Laepple, M. Furthmeier, E. Dardanis, N. Dessmann, L. Li, E. H. Linfield, A. G. Davies, M. S. Vitiello, and R. Huber, "Ultrafast two-dimensional field spectroscopy of terahertz intersubband saturable absorbers," Opt. Express **27**, 2248 (2019).